***Research Article***

Chemical Review and Letters
journal homepage: www.chemrevlett.com
ISSN (online): 2645-4947 (print) 2676-7279

# A Novel Method for Nanocrystallization of Nanostructured Materials for Radiation Exposure Measurements

Kaivalya Gupta[1], Gayatri Verma[2] Ratnesh Tiwari[3], Amit Kumar Beliya[4], Sujit kumar Shende[5]

[1]*Department of Physics, CV Raman University Bilaspur, Kota, C.G., India*
[2]*Department of Physics, CV Raman University Bilaspur, Kota, C.G., India*
[3]*Professor, Department of Physics, CV Raman University Bilaspur, Kota, C.G., India*
[4]*Assistant Professor Government Chandra Vijay College Dindori (MP), India*
[5]*Raja Shankar Shah University Chhindwara(MP), India*

ARTICLE INFO

*Article history:*
Received 3 March 2024
Received in revised form 1 April 2024
Accepted 2 April 2024
Available online 26 April 2024

*Keywords:*
Nanocrystallization,
Nanomaterials,
Radiation
Phosphorus
Luminescent

ABSTRACT

Nanocrystallization processes of inorganic and biological materials yield a wide range of electrical, optical, and structural properties. This process focuses specifically on the potential of certain elements as fluorophores and unique host materials. These elements have unique properties, especially luminescence, which depends on their size. It occurs when impurities are added to the framework that limit quantum effects. The results of innovative research on the thermoluminescence (TL) properties of nanostructured materials are very promising. In this work, we aim to create high-performance materials to improve radiation exposure measurement instruments. In this paper, we report on the thermoluminescent properties of self-agglomerated $CaSO_4$:Samarium (Sm) samples prepared using an environmentally friendly coprecipitation method. Unlike conventional techniques, no additional binder is required to create solid $CaSO_4$:Sm samples. When subjected to beta particle irradiation, these materials exhibit peak TL intensity at 490 K at a heating rate of 4.8 K/s. It exhibits twice the sensitivity of the TLD-100 dosimeter already on the market. Additionally, the minimum detection level for these samples was found to be less than 0.71mGy.The investigation shows that computerized glow curve decomposition, as part of the residual emission curve fitting approach created by McKeever, shows that the emission curve is composed of four separate TL peaks exhibiting intermediate-order motion.

## 1. Introduction

The fields of materials science, biotechnology, and genetics have all shown significant interest in nanoscience and nanotechnology [1-14]. In recent years, the importance of nanomaterials in the field of luminescence has increased significantly due to their improved optical, electrical, and structural properties [15-16]. These materials have shown potential as effective phosphors in a variety of display applications, including flat panel displays powered by low-energy sources, solar energy conversion systems, optical amplifiers, and TLD phosphors. Over the past two decades, various new physical and chemical synthesis techniques have been developed to facilitate the production of nanoparticles and nanorods using different ceramic materials [17-18]. Furthermore, recent studies have shown that factors such as shape, size, incorporation of impurities at various locations, and the presence or absence of specific defects can influence the optical, luminescent, and other relevant properties of these nanomaterials. It was revealed how it affects.

∗ Corresponding author: e-mail: 31rati@gmail.com
https://doi.org/10.22034/crl.2024.446784.1304

Thermoluminescence (TL), also known as thermally stimulated luminescence, is a powerful technique commonly used to determine ionizing radiation exposure. The main components used in TL dosimeters (TLDs) are primarily inorganic crystalline materials, commonly available in chip, single crystal, or microcrystalline dimensions [19-20]. TL is a widely used and highly reliable method for measuring ionizing radiation that utilizes inorganic crystalline minerals as its dosimeter. These are known as thermoluminescence dosimeters (TLDs). These materials exist as single crystals, chips, or microcrystalline powders and have the important function of accurately monitoring radiation administration. Recent advances in TL research have revealed the significant potential of nanomaterials in this field, demonstrating properties such as improved sensitivity and saturability at high doses [21-22]. Additionally, research on glowing ceramic micro- or nanoparticles has revealed promising applications in radiation measurements, such as medical imaging, high-energy physics, and non-destructive testing. Over the past two decades, there has been a significant increase in the idea of using various ceramic materials as radiation detectors [22-24]. This illustrates the changing landscape of TL technology and its increasing scope of applications.Current TLD materials consist of inorganic crystalline compounds called phosphates. These materials have the ability to emit visible light radiation when properly stimulated. These are commonly found in several forms, including chips, single crystals, or microcrystalline powders. Several commercially available top-level domains accomplish this purpose under different brand identities. Some of the best-known examples are LiF:Mg, Ti (TLD-100), LiF:Mg, Cu, P (TLD-700H), $CaF_2$:Dy (TLD-200), $CaSO_4$:Dy (TLD - 900), $Al_2O_3$:C (TLD-500) (Table 1). The research focuses s. on the thermoluminescence (TL) properties of LiFnanocubes when exposed to gamma rays and $C^{6+}$ ions. Specifically, samples doped with Eu and Tb have been shown to be particularly sensitive among the mentioned samples [22-27]. The dosimetric performance of $Al_2O_3$ nanoparticles has been investigated with respect to their response to gamma rays and $C^{6+}$ ions at 85 MeV. Experiments show a particularly consistent response and little fading of the TL in the Tb-doped sample.Research shows the formation of nano- and micro-sized $CaSO_4$ particles and investigates how different dopants (Tb, Dy, and Eu) affect their thermoluminescent properties after exposure to gamma rays it was done. Samples containing Eu and Tb exhibit distinctive TL peaks at 250–270 °C [28]. These samples show direct dose correlation in the range 12 Gy to 11 kGy. These properties make it a particularly ideal phosphor for high-dose dosimetry applications such as food and seed irradiation.The process of creating $CaSO_4$:X typically uses sulfuric acid, which carries considerable health risks [29]. Pratik and colleagues introduced their work on improving a new high-sensitivity phosphor called CaSO4:Dy,Mn, describing in detail its development and characterization process. They used traditional recrystallization methods to synthesize CaSO4:Dy,Mn. To analyze their properties, they performed thermoluminescence (TL) studies, exposing the phosphors to gamma radiation emitted from Cs-137 at doses ranging from 10 µGy to 100 Gy [15]. This health risk must be carefully considered. Additionally, this process causes damage to the environment. For practical applications, solid-state dosimeters are preferred over powder-based ones. $CaSO_4$ is encapsulated in Teflon or glass to create a solid sample that is easy to handle, but this process prevents the production of pure $CaSO_4$ sample

**Table 1.** General attributes of some industrially accessible thermoluminescent dosimeters significant for particular dosimetry[22-29]

| TLD Type | Effective Atomic Number Zeff | Main Peak ($^0$C) | Emission Maximum (Nm) | Relative Sensitivity | Fading for storage in dark | Useful dose range |
|---|---|---|---|---|---|---|
| LiF: Mg,Ti | 8.4 | 210 | 410 | 1 | 5% / year | 20 µGy-10 Gy |
| LiF: Mg,Cu,P | 8.4 | 220 | 410 | 28 | 5% / year | 0.2 µGy-10 Gy |
| $Li_2B_4O_7$:Cu | 7.6 | 210 | 378 | 2 | 10% / 2 month | 10 µGy 10Gy |
| $MgB_4O_7$:Dy | 8.6 | 200 | 495 | 12 | 4%/ month | 5 µGy-50 Gy |
| $Mg_2SiO_4$:Tb | 12 | 210 | 390-410 | 45 | Negligible | 10 µGy 1Gy |
| $CaSO_4$:Dy | 15.6 | 230 | 490-580 | 35 | 1%/2 month | 2 µGy- 10 Gy |
| $CaSO_4$:Tm | 15.6 | 230 | 462 | 40 | 1.2%/2 months | 2 µGy- 10 Gy |

| | | | | | | |
|---|---|---|---|---|---|---|
| $Al_2O_3$:C | 10.4 | 200 | 430 | 65 | 5%/ year | 1 µGy- 10 Gy |
| $CaSO_4$:Sm (This work) | 15.1 | 210 | 490 | 67 | 2%/Year | 0.07 -1.0Gy. |

In this work, our goal is to create sophisticated materials that improve the functionality of radiation exposure measuring systems. These materials are designed to provide increased sensitivity, consistency, low moisture absorption, and a strong reaction to both radiotherapy and mixed radiation settings. In order to do this, we investigated the thermoluminescence properties of self-aggregated $CaSO_4$:Sm samples irradiated with β particles. We considered several factors, including TL response to irradiation dose, sensitivity in terms of a number of irradiation-TL readout cycles, lowest detection limit, and TL fade. Furthermore, computerized emission curve analysis using a generalized order kinetics model reveals that the emission curve has four distinct peaks, among which the order of the main peak is b = 1.47.

## 2. Experimental

Various Sm-doped $CaSO_4$ materials were prepared using a solid-state reaction method. The dopant concentration was varied from 0.02 to 12 mol% of Sm. The synthesis technique involved carefully mixing the powdered reagents $CaSO_4$·0.5H2O (purity ≥99%) and Sm2O3 : Sm (purity ≥99.9%) using a toast and pestle. The well-mixed mixture was then placed into an $Al_2O_3$ crucible. The crucible containing this combination was heated to 1200 °C for 4 hours in an ambient air environment in a Yamada Electric electric furnace model ETSS-430.After mixing, the produced mixture was put into an $Al_2O_3$ crucible for heating. The crucible served as a vessel that provided consistent heating and reduced material loss throughout the heat treatment process. The decision to use $Al_2O_3$ in the crucible was intentional due to its high-temperature stability and inert properties. These properties are essential to preserve the integrity of the reaction environment. The filled crucible was then subjected to a regulated heating schedule with an electric boiler. The heating procedure was carried out at a temperature of 1200 °C for 4 h under normal air conditions. A prolonged heat treatment progressively converted the precursor mixture into the intended Sm-doped $CaSO_4$ compound via a solid-state reaction process. During heating, precise temperature control was maintained to achieve proper phase composition and structural integrity of the composite material. Figure 1 shows the pictorial representation of synthesis of $CaSO_4$

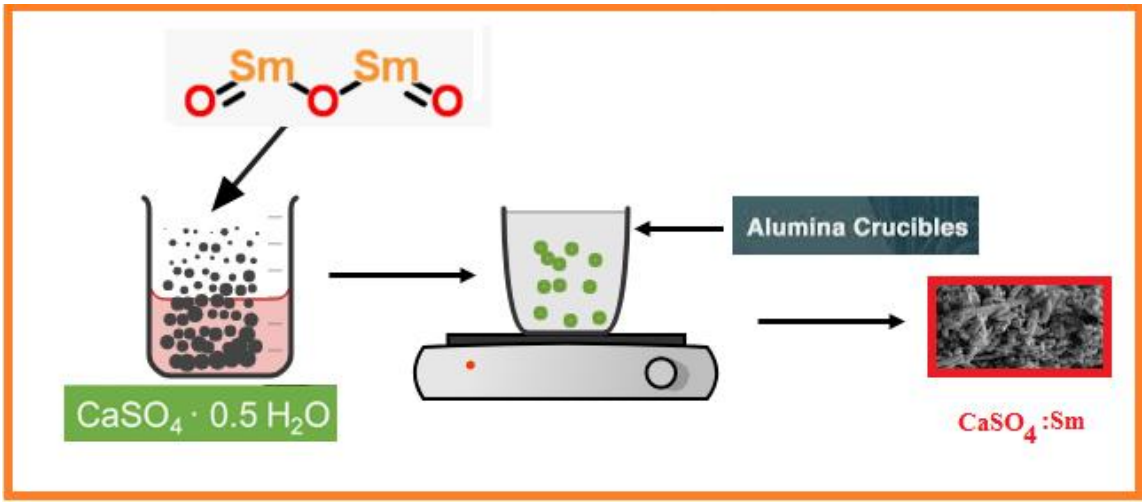


**Fig. 1.** Experimental process to synthesis $CaSO_4$:Sm

## 3. Important Performance parameter

Systems that undergo electrical or fundamental changes to enable optical reading of radiation exposure are called optical storage phosphors or materials. These fluorophores emit light, have stable or substablecenters, and can be read many times by optical excitation. The main recombination pathway uses impurity integration to transition from surface states to impurity states. The radiative efficiency of impurity-induced emission increases as the confinement of impurity-induced changes to transition metals or rare earth elements increases.

Radiometric properties that influence phosphor performance and future applications include the investigation of thermoluminescence emission curves, TL emission spectra, dose-response, fading behavior, reproducibility, and reusability [30].

**Glow Curve**

In radiotherapy measurements, different thermoluminescence properties must be considered when selecting a radiation dosimetry device for radiotherapy measurements. Adjustment of radiation dose estimation and radiation exposure field ensures adequate accuracy within the required medium and creates a favorable characteristic relationship between accuracy and dosimeter response, as well as linearity between radiation dose and response; Sensitivity to the signal and TL emission curve must be evaluated. In addition, the suitability of the system for monitoring and evaluation of radiation applications is evaluated by careful investigation and validation of specific parameters.

**TL Glow Curve**

The shallow traps closest to the conductive band empty quickly at room temperature, causing discernible TL signal attenuation. On the other hand, radiometric traps require a slightly higher energy input to release the trapped electrons, which is usually the key indicator for radiometric analysis and forms a peak in the TL output. High temperature annealing is a useful technique for emptying deeply buried traps that require significant amounts of energy. As a result, the maximum peak intensity of TL increases with radiation exposure.

**TL Response**

Thermoluminescent dosimeters are characterized by a linear relationship between TL (thermoluminescent) radiation and absorbed dose. This correlation is essential for accurate radiation dosimetry. Certain thermoluminescent materials have a noticeable effect on various linearities, ensuring accurate readings. Typically, the response of TL phosphors shows a linear trend at low doses, transitions to superlinear at intermediate doses, and finally reaches saturation at high doses

## 4. Results and Discussion

Figure 2 shows the peak intensities of TL emission after $CaSO_4$: Sm samples with different iodine concentrations (0.2, 0.4, 1.0, and 1.2mol%) were exposed to 2.5 Gy of beta particle irradiation. This irradiation setting was chosen to reproduce authentic environmental exposure situations. The sample containing 4.5 mol% Sm showed the strongest TL emission, thus suggesting its potential in applications requiring radiation dosimetry and fluorescence properties for displays and sensors. Therefore, samples containing this specific Sm concentration were selected to ensure the best performance and consistency in future characterization. Additional investigations were conducted to further the investigation and explore the chemical composition and function of potassium iodide in the $CaSO_4$ matrix. Photoluminescence spectroscopy was used to confirm the presence of iodine in the sample and determine its oxidation state.

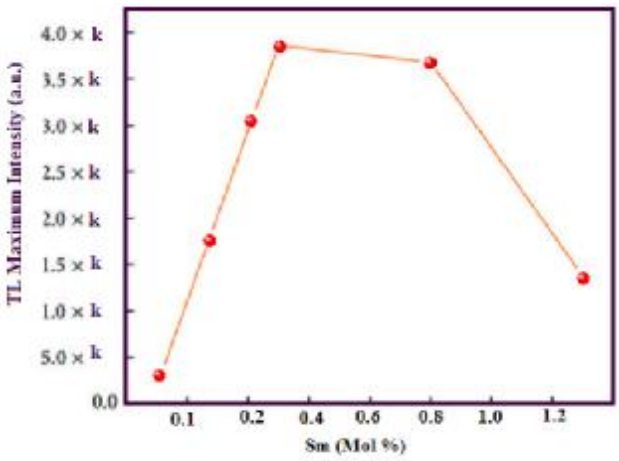


**Fig. 2**: Peak intensities of TL emission after $CaSO_4$: Sm samples with different Sm concentrations

Figure 3 shows the photoluminescence emission spectrum produced by activating the synthesized $CaSO_4$: Sm sample with 394 nm light. The excitation wavelength was intentionally chosen to match the absorption peak of iodine ions.

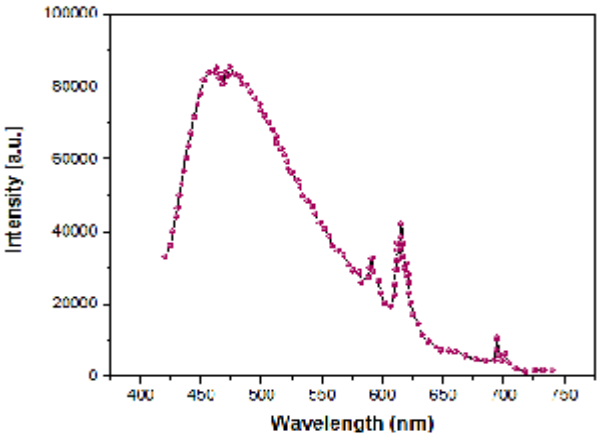


**Fig. 3.** Photoluminescence emission spectrum produced by activating the synthesized $CaSO_4$: Sm

This ensured effective excitation and accurate emission signal detection.Distinct peaks at 587, 620, and 702 nm in the PL (fluorescence light) emission spectrum indicate the emission of photons by iodine ions in the $CaSO_4$ matrix. The emission peak indicates the transition that occurs within the energy level of the $Sm^{3+}$ ions in the sample, indicating the presence of $Sm^{3+}$in the sample. The location and intensity of the emission peaks provide important information about the interaction of the iodine ion with its surrounding environment and host lattice.

Figure 4 shows the optical Glow curves of $CaSO_4$:Sm when the beta particle irradiation dose was varied between 0.07 and 1.0Gy. The graph clearly shows that multiple glow curves appear and the intensity of the TL increases at higher doses. Experiments also included larger doses reaching up to 180Gy, which will be discussed later. Surprisingly, there was no significant change in the maximum value of TL.The view factor calculated by analyzing the light curve peaks is 0.46, close to the expected value of 0.41, indicating a first-order process. The modest deviation from the predicted values suggests the presence of many individual peaks and/or the influence of non-linear kinetically ordered TL processes.The TL peak, located at around 476.15 K, has potential for dosimetry applications. Less pronounced peaks may also be seen at 444.23 K and above 777.31 K, enhancing the understanding of $CaSO_4$:Sm 'sthermoluminescence properties in different situations.

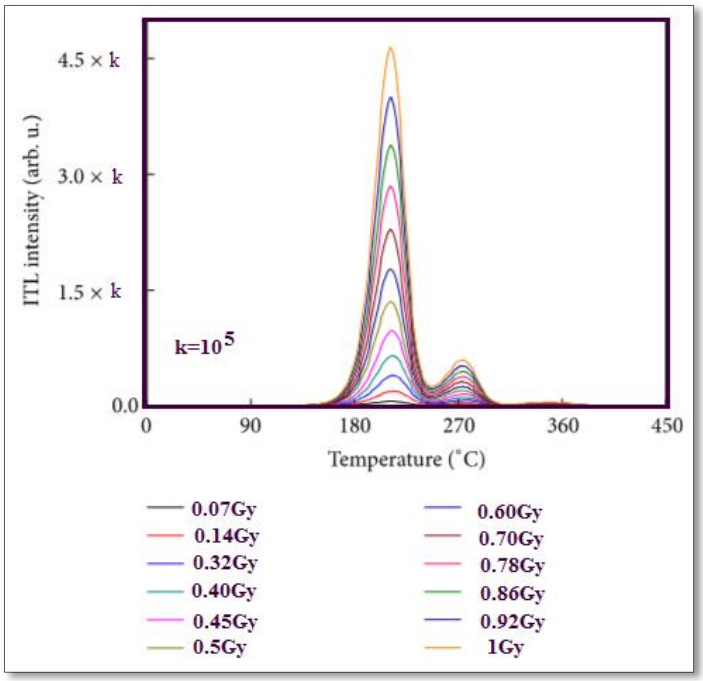


**Fig. 4.** optical Glow curves of $CaSO_4$: Sm when the beta particle irradiation dose was varied between 0.07 and 1.0Gy.

Figure 5(a) shows the integrated TL (ITL) associated with beta particle irradiation from 0.07 to 1Gy. Figure 5(b) shows the behavior of the ITL for doses up to 130Gy. An interesting pattern is observed, with a superlinear trend at smaller doses, but a sublinear relationship observed at doses above 11Gy with signs of saturation above 53Gy. The lowest detection limit (LDL) is 0.68mGy and depends on the sample and the reading device used. Although LDL values were calculated and showed a linear dependence at low doses, the method used to irradiate the samples cannot deliver doses below 84mGy. Further studies are needed to study the TL properties of $CaSO_4$ synthesized at low doses, and its response to different radiation doses should be thoroughly investigated.

Figure 6 shows the correlation between integrated TL (ITL) and post-irradiation TL reading interval. The TL signal shows impressive consistency across the observed period. Exposure to radiation reduces the initial integrated TL by 2.4% when the samples are stored in the dark at room temperature.

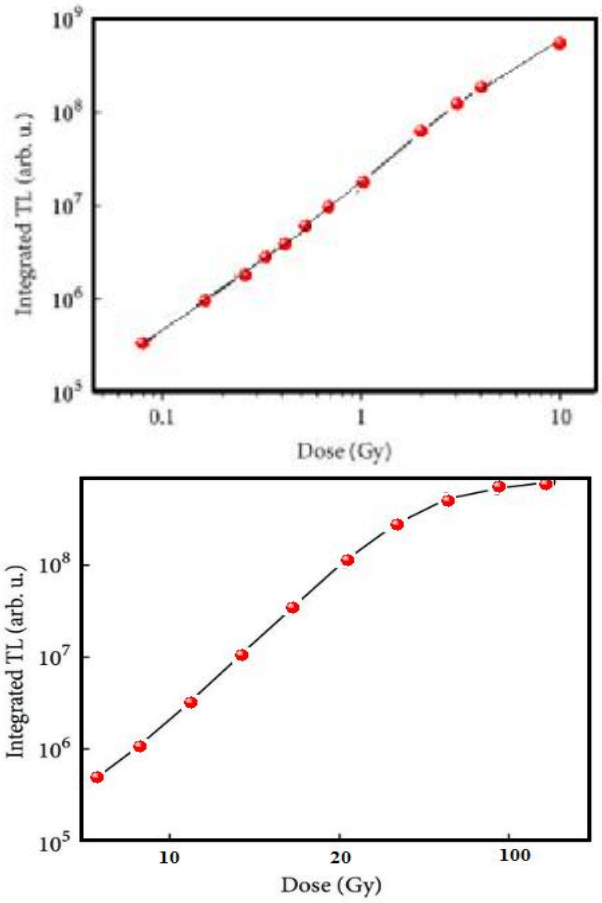


**Fig. 5.** Integrated TL associated with beta particle irradiation with respect to radiation dose

All samples were uniformly exposed to 1.0 Gy of beta particle irradiation. This continuous behavior indicates the reliability of the TL signal over different time intervals and exposure situations.

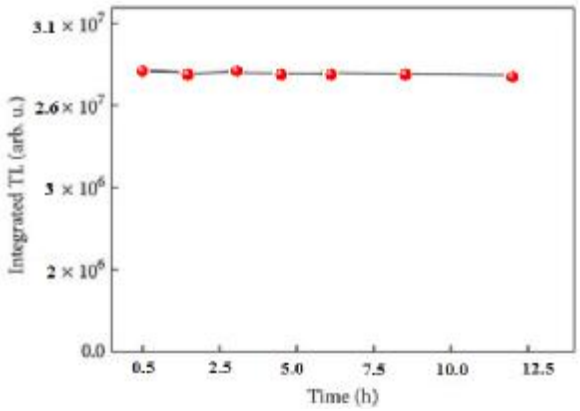


**Fig. 6**. Correlation between integrated TL (ITL) and post-irradiation TL reading interval

Figure 7 shows the relationship between $T_M$ and $T_{STOP}$(K) using a graph created by recording the first TL maximum associated with the glow curve after partial cleaning to a specific temperature. The graph shows three distinct peaks that match the light curve shown in Figure 4. Figure 4 shows a stable peak position regardless of dose changes, whereas the curvature of the step in Figure 8 indicates the presence of a non-linear response. This computational process begins by analyzing the residual emission curve associated with the highest $T_{stop}$ temperature, aiming to isolate the most prominent TL peak and accurately assess its capture parameters. After accurately determining these parameters, the next step is to resolve the residual emission curves associated with lower Tstop temperatures. This process involves resolving subsequent individual peaks while maintaining the best peak kinetic parameters.

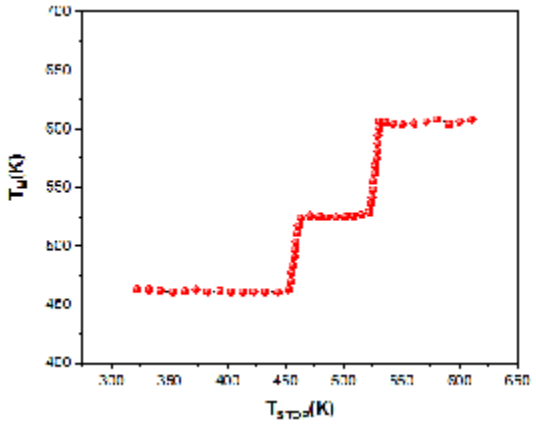


**Fig. 7.** Relationship between $T_M$ and $T_{STOP}$(K)

Figure 8 show the configuration of the glow curves at temperatures of 543 K. These curves show different TL peaks, such as the high-temperature TL peak at 643 K seen in Fig. 8 and the main and satellite peaks located at lower temperatures.

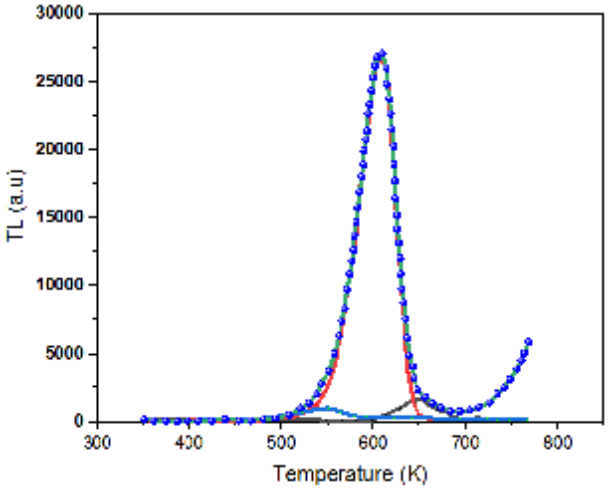


**Fig. 8.** Glow curves at temperatures of 543 K

## 5. Conclusion

This study investigates the thermoluminescent properties of self-aggregated $CaSO_4$:Sm upon exposure to beta particle radiation. The synthesized $CaSO_4$ exhibits self-aggregation ability, eliminating the need for additional binding elements in creating 100% $CaSO_4$:Sm solid samples. The synthesis of $CaSO_4$ is a simple and economical technique that involves an ecologically favorable chemical process.The pelleted sample exhibits a pronounced thermoluminescence (TL) peak at 200 °C when heated at a rate of 5 °C/s. The sample is twice the sensitivity of the TLD-100 dosimeter currently on the market, with a detection threshold of less than 1.0 mGy. Although this study focuses on beta particle exposure, previous studies mentioned in Section 1 have shown that different forms of radiation can also cause thermoluminescence in $CaSO_4$.Computerized emission curve analysis showed that the residual emission curve from the McKeever test was composed of four discrete peaks with intermediate-order kinetics. This detailed analysis has improved our knowledge about the thermoluminescence properties of CaSO4:Sm when exposed to β-particle radiation, opening its potential applications in dosimetry and radiation detection in different regions.

**References**


[1] A. K. O. Aldulaim, N. M. Hameed, T. A. Hamza, A. S. Abed, The antibacterial characteristics of fluorescent carbon nanoparticles modified silicone denture soft liner. J. Nanostruct., 12 (2022) 774-781. doi:10.22052/JNS.2022.04.001.

[2] P. O. Ameh, Removal of Methylene Blue from Aqueous Solution using Nano Metal Oxide Prepared from Local Nigerian Hen Egg Shell: DFT And Experimental Study, Chem. Rev. Lett. 6 (2023) 29-43. 10.22034/crl.2023.328721.1155

[3] E. Vessally, M.R. Ilghami, M. Abbasian, Investigation the Capability of Doped Graphene Nanostructure in Magnesium and Barium Batteries with Quantum Calculations, Chem. Res. Technol. 1 (2024). 10.2234/chemrestec.2024.436837.1007.

[4] B. Baghernejad, F. Nuhi, A new approach to the facile synthesis of 1,8-dioxooctahydroxanthene using nano-TiO2/ CNT as an efficient catalyst, Chem. Rev. Lett. 6 (2022) 268-277. 10.22034/crl.2022.340828.1166

[5] P. O. Ameh, Synthesized iron oxide nanoparticles from Acacia nilotica leaves for the sequestration of some heavy metal ions in aqueous solutions, J. Chem. Lett. 4 (2023) 38-51. 10.22034/jchemlett.2023.360137.1083.

[6] H. Ashassi-Sorkhabi, A. Kazempour, J. Mostafaei, E. Asghari, Impact of ultrasound frequency on the corrosion resistance of electroless nickel-phosphorus-nanodiamond plating, Chem. Rev. Lett. 6 (2022) 187-192. 10.22034/crl.2022.345098.1169

[7] Milad. Sheydaei, M. Edraki, Poly(butylene trisulfide)/CNT nanocomposites: synthesis and effect of CNT content on thermal properties, J. Chem. Lett. 3 (2022) 159-163. 10.22034/jchemlett.2023.380990.1101.

[8] B. Ghanavati, A. Bozorgian, J. Ghanavati, Removal of Copper (II) Ions from the Effluent by Carbon Nanotubes Modified with Tetrahydrofuran, Chem. Rev. Lett. 6 (2022) 68-75. 10.22034/crl.2022.326950.1152

[9].M. Sheydaei, M. Edraki, Vinyl ester/C-MMT nanocomposites: investigation of mechanical and antimicrobial properties, J. Chem. Lett. 3 (2022) 95-98. 10.22034/jchemlett.2022.350678.1074.

[10] M. Sheydaei, S. Shahbazi-Ganjgah, E. Alinia-Ahandani, M. Sheidaie, M. Edraki, An overview of the use of plants, polymers and nanoparticles as antibacterial materials, Chem. Rev. Lett. 6 (2022) 207-216. 10.22034/crl.2022.343015.1168

[11] P. R. A. Selvan, M. Praveendaniel, Synthesis and Application of TiO2-Phosphomolybdic acid nanocomposite, J. Chem. Lett. 4 (2023) 10.22034/jchemlett.2023.395693.1114.

[12] S. Arabi, Adsorption of Orange 3R by chitosan modified montmorillonite nanocomposite, Chem. Rev. Lett. 6 (2023) 55-65. 10.22034/crl.2023.387842.1208.

[13] C.P. Vardhani, STRUCTURAL AND OPTICAL PROPERTIES OF (MgZnO/rGO) NANOCOMPOSITES, J. Chem. Lett. 4 (2023) 10.22034/jchemlett.2023.396420.1116

[14] S. Bahl, S. Lochab, P. Kumar, CaSO4: Dy, Mn: A new and highly sensitive thermoluminescence phosphor for versatile dosimetry, Radiation Physics and Chemistry 119 (2016) 136-141.

[15] F. Daniels, C.A. Boyd, D.F. Saunders, Thermoluminescence as a research tool, Science 117 (1953) 343-349.

[16] T. Yamashita, N. Nada, H. Onishi, S. Kitamura, Calcium sulfate activated by thulium or dysprosium for thermoluminescence dosimetry, Health physics 21 (1971) 295-300.

[17] K. Nambi, V. Bapat, A. Ganguly, Thermoluminescence of CaSO4 doped with rare earths, Journal of Physics C: Solid State Physics 7 (1974) 4403.

[18] B. Dhabekar, S. Menon, R. Kumar, T.G. Rao, B. Bhatt, A. Lakshmanan, Electron spin resonance and thermoluminescence studies in CaSO4: Dy, Ag phosphor, Journal of Physics D: Applied Physics 38 (2005) 3376.

[19] K.K. Gupta, R. Kadam, N. Dhoble, S. Lochab, V. Singh, S. Dhoble, Photoluminescence, thermoluminescence and evaluation of some parameters of Dy3+ activated Sr5 (PO4) 3F phosphor synthesized by sol-gel method, Journal of Alloys and Compounds 688 (2016) 982-993.

[20] A. Kadam, G.C. Mishra, S. Dhoble, Thermoluminescence study of Eu3+ doped Na2Sr2Al2PO4Cl9 phosphor via doping of singly, doubly and triply ionized ions, Ceramics International 46 (2020) 132-155.

[21] V.E. Kafadar, T. Yeşilkaynak, R.E. Demirdogen, A.A. Othman, F.M. Emen, S. Erat, The effect of Dy3+ doping on the thermoluminescence properties of Ba2SiO4, International Journal of Applied Ceramic Technology 17 (2020) 1453-1459.

[22] T. Lyu, P. Dorenbos, Vacuum-referred binding energies of bismuth and lanthanide levels in ARE (Si, Ge) O4 (A= Li, Na; RE= Y, Lu): toward designing charge-carrier-trapping processes for energy storage, Chemistry of Materials 32 (2020) 1192-1209.

[23] M.K. Biroon, M. Zahedifar, E. Sadeghi, F. Almasifard, Preparation, kinetic analysis and thermoluminescent dosimetry features of highly sensitive SrF2: Dy phosphor, Radiation Physics and Chemistry 159 (2019) 1-5.

[24] U. Madhusoodanan, M. Jose, A. Lakshmanan, Development of BaSO4: Eu thermoluminescence phosphor, Radiation measurements 30 (1999) 65-72.

[25] N. Salah, P. Sahare, S. Lochab, P. Kumar, TL and PL studies on CaSO4: Dy nanoparticles, Radiation Measurements 41 (2006) 40-47.

[26] N. Ingle, S. Omanwar, P. Muthal, S. Dhopte, V. Kondawar, T. Gundurao, S. Moharil, Synthesis of CaSO4: Dy, CaSO4: Eu3+ and CaSO4: Eu2+ phosphors, Radiation measurements 43 (2008) 1191-1197.

[27] A. Pandey, S. Bahl, K. Sharma, R. Ranjan, P. Kumar, S. Lochab, V. Aleynikov, A. Molokanov, Thermoluminescence properties of nanocrystalline K2Ca2 (SO4) 3: Eu irradiated with gamma rays and proton beam, Nuclear Instruments and Methods in Physics Research Section B: Beam Interactions with Materials and Atoms 269 (2011) 216-222.

[28] R.C. Satkar, A.R. Kadam, D.A. Ovhal, S. Dhoble, Inorganic thermoluminescent phosphors in radiation dosimetry: An overview, Journal of Physics: Conference Series, IOP Publishing, 2021, pp. 012023.
[29] S.J. Dhoble, V. Chopra, V. Nayar, G. Kitis, D. Poelman, H.C. Swart, Radiation dosimetry phosphors: synthesis, mechanisms, properties and analysis, Woodhead Publishing2022.
[30] M. Singh, P. Sahare, Redox reactions in Cu-activated nanocrystalline LiF TLD phosphor, Nuclear Instruments and Methods in Physics Research Section B: Beam Interactions with Materials and Atoms 289 (2012) 59-67.